Journal of Biomolecular NMR, **15:** 189–201, 1999.
KLUWER/ESCOM

Water-macromolecule interactions by NMR: A quadrature-free constant-time approach and its application to CI2

Giuseppe Melacini, Rolf Boelens & Robert Kaptein*
NMR Department, Bijvoet Center for Biomolecular Research, Utrecht University, P.O. Box 80.075, NL-3508 CH Utrecht, the Netherlands

Received 11 June 1999; Accepted 25 August 1999

Key words: CI2, chemical exchange, constant-time, hydration, lysozyme, NOE, quadrature detection, ROE, water, water flip-back

Abstract

A pulse sequence is proposed to select water magnetization with enhanced specificity through a synergetic combination of several filtering principles. This approach relies on a constant-time evolution period implemented without quadrature detection, which results in a $\sqrt{2}$ increase in signal-to-noise ratios as compared to traditional non-selective methods for water filtration. In addition, the quadrature-free constant-time block facilitates the implementation of the water flip-back strategy, which leads to further gains in sensitivity. The proposed experiment was applied to unlabeled HEW lysozyme and to ^{15}N-labeled chymotrypsin inhibitor 2 which was partially or non ^{13}C-enriched. Water molecules belonging to a spine of hydration between two pseudo β-sheet strands were identified, solving previously reported discrepancies between the X-ray and the refined NMR structure of CI2. The proposed experiment is particularly suitable for hydration studies of mixtures of labeled and unlabeled components, such as ligand–macromolecule complexes.

Introduction

Problem definition

High resolution nuclear magnetic resonance spectroscopy is an important tool to characterize the localization and the exchange kinetics of water molecules bound to biological systems (Pitner et al., 1974; Otting and Wüthrich, 1989; Otting et al., 1991a; Otting, 1997). The NMR experiments designed to investigate macromolecule–water interactions are generally composed of three major building blocks. First, the water magnetization is selected while the biomolecule magnetization is discarded. Second, magnetization is transferred from water to macromolecular protons. Third, these protons are properly frequency labeled in one or two homo- or heteronuclear dimensions. This paper focuses on the first step: selection of the water signal.

*To whom correspondence should be addressed. E-mail: kaptein@nmr.chem.uu.nl

Most methods select water magnetization primarily based on its resonance frequency by using non-selective frequency labeling (Otting and Wüthrich, 1989; Otting et al., 1991b; Otting, 1994; Sklenar, 1995) or by selective water excitation via 90° (Mori et al., 1994, 1996a,b; Otting and Liepinsh, 1995a,b; Liepinsh and Otting, 1999) or 180° pulses (Dalvit, 1995, 1996; Dalvit and Hommel, 1995a,b; Otting and Liepinsh, 1995a; Böckmann and Guittet, 1996). These schemes have been optimized to select only a narrow frequency band centered on the water signal, but they cannot filter out magnetization arising from macromolecular protons resonating as well within the selected band (i.e. the $C^{\alpha}H$ protons of proteins). Additional physical properties other than the resonance frequencies must then be exploited to differentiate between biomolecular and water proton magnetization. Specifically, isotope filters based on heteronuclear coupling constants are very effective in suppressing the ^{13}C-labeled macromolecular components of the solution (Gemmecker et al., 1993; Grzesiek and Bax,

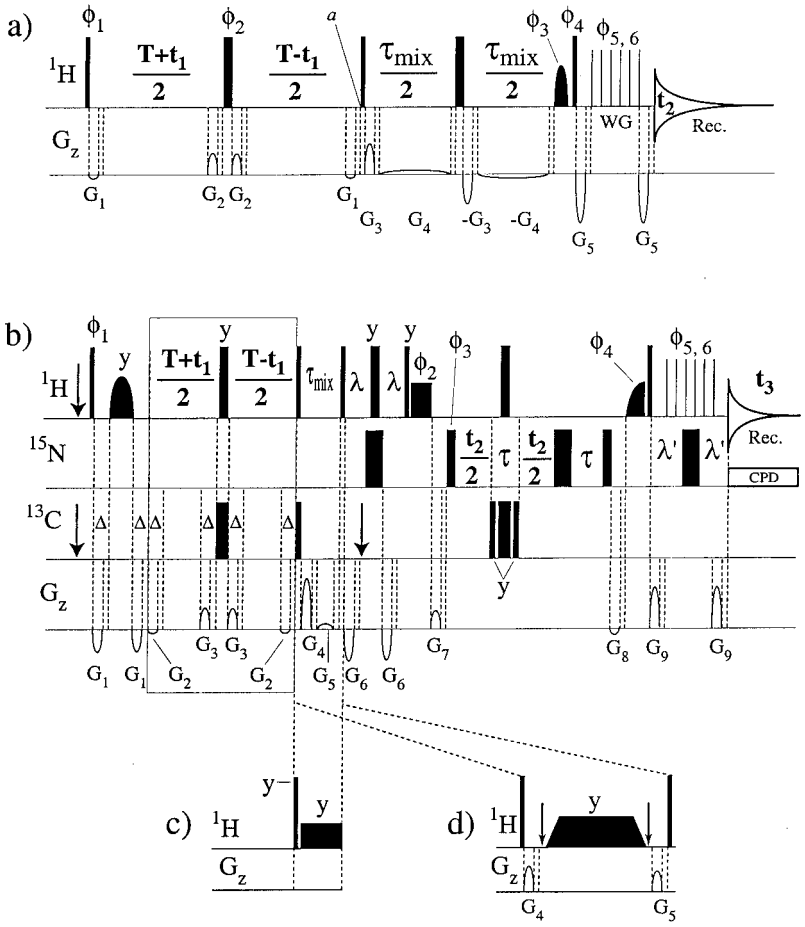

1993a,b; Karimi-Nejad et al., 1999). However, proteins may only be partially labeled and/or the solution may contain a complex of labeled and unlabeled molecules. In these cases, the magnetization of the unlabeled biomolecular components can be filtered out by exploiting further properties such as diffusion rates, homonuclear scalar coupling constants and transverse relaxation, as demonstrated in several recently published elegant pulse sequences (Kriwacki et al., 1993; Mori et al., 1996b; Wider et al., 1996). Here, it is shown how these different selection strategies can be synergistically combined in a constant-time (CT) t_1-evolution block (Bax et al., 1979; Bax and Freeman, 1981; Rance et al., 1984; Santoro et al., 1992; van de Ven and Philippens, 1992; Vuister and Bax, 1992) (Figure 1) resulting in a filter with enhanced specificity for water magnetization.

Methods

The combined constant-time (CT) filter – conceptual basis

At the end of the CT block of length T (point *a* in the sequence of Figure 1a), the relevant magnetization for proton I of a generic isotropically diffusing biomolecule is described by (Santoro et al., 1992; van de Ven, 1995; Cavanagh et al., 1996; Wider et al., 1996):

$$-I_y f \cos(\Omega_I t_1)[\Pi_k \cos(\pi J_{ik} T)] \exp(-T/T_2^i) \exp(-\gamma^2\tau^2 G^2 (T-\xi) D) \quad (1)$$

where $f = \exp(-t_1/T_{2inhom}) \sim 1$, T_{2inhom} is the small inhomogeneous contribution to the total transverse relaxation rate $1/T_2^{i*} = 1/T_2^i + 1/T_{2inhom}$ and the J_{ik} indicate homonuclear coupling constants between protons I (i.e. an α-proton) and K (i.e. amide and β-protons); γ is the gyromagnetic ratio for protons, τ and G are, respectively, the length and strength of the gradients bracketing the CT period (G_1 in Figure 1a

Figure 1. Pulse sequences to measure dipolar cross-relaxation and/or chemical exchange rates between water and macromolecular systems which are unlabeled (a) or which are ^{15}N-labeled and partially or non ^{13}C-labeled (b–d). For all experiments and all nuclei thin and thick bold vertical bars represent 90° and 180° hard pulses, respectively, and the WATERGATE (WG) block is implemented using the 3-9-19 pulse train (Sklenar et al., 1993). The proton carrier frequency used during the CT period is always set on the middle of the water resonance as explained in the text. T is the total duration of the CT-t_1 evolution period and if a ^{13}C-labeled component is present, in sequences (b-d) $T = \sigma\ (1+2n)$, where $\sigma = (1/2^1J_{13C^\alpha H^\alpha})$ and n is a positive integer. Gradients are always followed by a delay of at least 0.2 ms and have a sinus amplitude profile with a duration of 0.5 ms, except for G_4 and G_5 in panels (a) and (b), respectively, which determine the length of the NOE mixing time (τ_{mix}). All phases are x unless otherwise specified. (a) Pulse sequence for the quadrature-free (QF) constant-time (CT) 2D-NOESY WG experiment. The 90° water flip-back (WFB) (Grzesiek and Bax, 1993b; Dalvit, 1996) has the shape of the center lobe of a sin(x)/x function and a duration of 2.144 ms (Grzesiek and Bax, 1993a). The relative strengths of the gradients are: G_1 −1.00, G_2 5.00, G_3 7.40, G_4 1.06, G_5 −30.00. Phases are: ϕ_1 = x, −x; ϕ_2 = 4(y), 4(−y); ϕ_3 = −x, x, x, −x; ϕ_4 = x, x, −x, −x; ϕ_5 = x; ϕ_6 = −x; ϕ_{Rec} = x, −x, −x, x. Quadrature detection (QD) is not needed because this experiment is dedicated to the measurement of water–protein interactions. The pulse sequence can therefore be written as for States-TPPI (Marion et al., 1989) but the 90° incrementation of the phase of the first pulse is eliminated. The receiver phase can be inverted when t_1 is incremented. (b) Pulse sequence for the 3D e-PHOGSY-QF-CT-soft-NOESY-WFB-HSQC experiment. The e-PHOGSY spin-echo at the beginning of the pulse sequence is implemented with a relatively short Gaussian pulse (4.04 ms) which allows to reduce SW(ν_1) to 1602.6 Hz, 'softening' the NOESY experiment. The QF-CT block is boxed. The WFB-HSQC is implemented essentially as described in the literature (Grzesiek and Bax, 1993a; Clore et al., 1994; Karimi-Nejad et al., 1999) with λ and λ' such that the total duration of the INEPT steps is $\leq 1/2J_{NH}$ (5 ms in the tested cases). In addition, the half-Gaussian pulse with phase ϕ_4 has a duration of 2.1 ms. The arrows in the ^{13}C channel indicate shifts of the ^{13}C channel carrier frequency: before the filter the ^{13}C carrier frequency is set at the middle of the C^α region, while after the filter and before the composite ^{13}C inversion pulse in the middle of ^{15}N evolution the ^{13}C carrier frequency is set at a value between the C^α and the C(O) regions (Karimi-Nejad et al., 1999). The ^{15}N 180° pulse at the end of t_2 eliminates the need for phase corrections in the ^{15}N dimension; however, if $t_{2,max}$ is short, the evolution of the ^{15}N-^{13}C couplings is insignificant and both the composite ^{13}C 180° pulse and the ^{15}N 180° pulse at the end of t_2 can be eliminated. The arrow in the ^{1}H channel indicates that the ^{1}H carrier frequency is set on water as explained in the text. The relative strengths of the gradients are: G_1 −6.20, G_2 −1.00, G_3 5.40, G_4 12.60, G_5 1.06, G_6 −7.40, G_7 3.15, G_8 −1.26, G_9 14.20. Minimal phase cycling is: ϕ_1 = x, −x; ϕ_2 = −x, x; ϕ_3 = x, x, −x, −x; ϕ_4 = −x; ϕ_5 = x; ϕ_6 = −x; ϕ_{Rec} = x, −x, −x, x. For t_1 no quadrature detection is employed similarly to experiment (a). In addition, ϕ_1, ϕ_2 and ϕ_{Rec} are inverted when t_1 is incremented. For t_2, quadrature detection is obtained using the States-TPPI method and no phase correction is necessary (Marion et al., 1989). The on-resonance and off-resonance ROE versions of the pulse sequence can easily be obtained modifying the NOE mixing block as shown in panels (c) and (d), respectively. The ^{15}N and ^{13}C pulses remain as in (b). For the on-resonance ROE experiment (c) phase cycling is like for the NOE sequence in (b) but ϕ_2 = x, −x. All ROE peaks are 180° out of phase as compared to the NOE peaks. A 25 ms spin-lock of 9.2 kHz was employed (Grzesiek and Bax, 1993a). For the off-resonance ROE experiment (d) the phases are as in the NOE version; however, the proton carrier is moved by an offset corresponding to $\theta = 35.5°$ (Birlirakis et al., 1996) before the spin-lock is applied (first arrow in panel (d)) and is brought back to the water frequency at the end of the locking period (second arrow in panel (d)). Summation of data acquired with positive and negative offsets is employed to minimize angular dispersion (Desvaux and Goldman, 1996). The spin-lock includes two 4 ms adiabatic pulses which scale up/down to/from a field of 7.8 kHz applied for 100 ms. Gradients are as for panel (b), but G_4 and G_5 are 13.4 and 12.6 (relative units, vide supra), respectively.

or G_2 in Figures 1b–d), $\xi = \Delta + (4\tau/3)$ where Δ is the stabilization delay following the gradients; finally, D is the translational diffusion coefficient of the macromolecule (Stejskal and Tanner, 1965).

Water magnetization is set to resonate at zero frequency offset, is not subject to scalar coupling and is usually characterized by a T_2 significantly larger than that of macromolecular protons when it is not broadened by chemical exchange with concentrated labile protons and it is dephased by gradients (see G_1 and G_2 in Figures 1a and b, respectively). Unless diffusion experiments are desired (vide infra), these gradients can be set weak enough to avoid diffusion losses of water magnetization while at the same time preventing radiation damping.

Clearly, the $\cos(\Omega_I\ t_1)$ term of Equation 1 encodes for the frequency filter, while the other cos terms encode for the homonuclear coupling filter and the first exponential term in T implements the relaxation filter. These three effects act simultaneously and cooperatively to select water magnetization. In addition, if the strength of the gradients applied at the beginning and at the end of the CT block is increased, the relatively faster diffusion of water molecules as compared to the macromolecule can be advantageously used to differentiate between intermolecular NOEs with water and intramolecular NOEs. The latter depend on the last term of Equation 1, as already previously described for spin-echos (Kriwacki et al., 1993; Wider et al., 1996). Here weak gradients will be employed (Figure 1) and therefore the focus will be on the other terms of Equation 1.

The longer the CT period (T), the more effective is the T_2 relaxation filter and the higher the allowed $t_{1,max}$, resulting in increased digital resolution. This feature is very appealing for frequency separation purposes considering that the macromolecular signals are not split by scalar couplings and that, since $t_{1,max}/T_{2inhom}$ is usually $\ll 1$, the lineshape of the signals in the frequency domain is mainly determined by

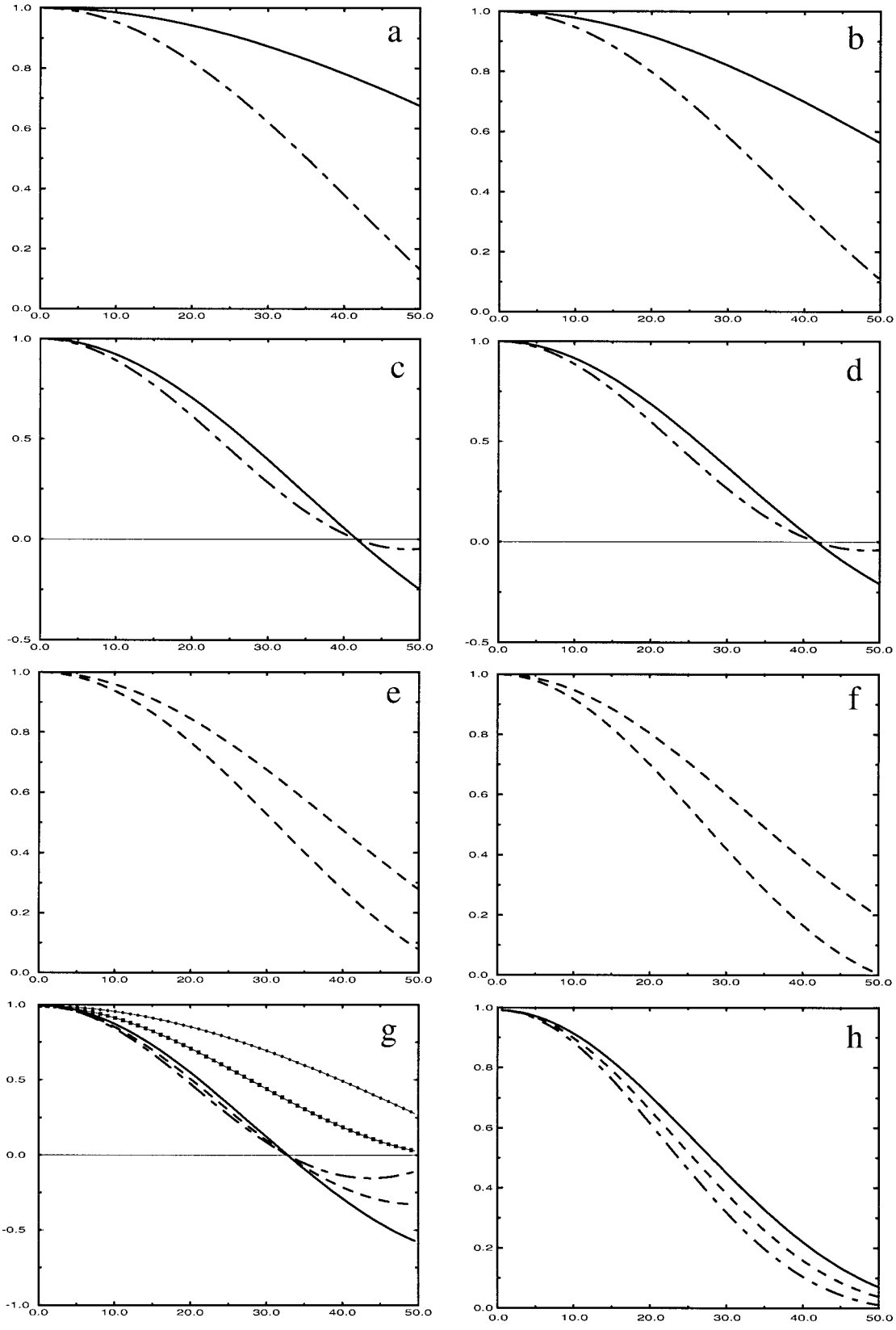
a
b
c
d
e
f
g
h
0.0
10.0
20.0
30.0
40.0
50.0

Figure 2. Plots of $\Pi_k \cos(\pi J_{ik} T)$ versus T, where T is the total duration (in ms) of the constant-time evolution period and $\Pi_k \cos(\pi J_{ik} T)$ represents the α-proton magnetization suppression factor obtained through homonuclear scalar coupling evolution of the α-protons with respect to couplings to amide and β-protons (see Equation 1) (Santoro et al., 1992; Mori et al., 1996b; Otting, 1997). The different plots refer to different representative conformations (Chakrabarti and Pal, 1998) and amino acid types. For all panels solid lines correspond to α-helices ($J_{H^\alpha H^N} \sim 4$ Hz), dot-dashed lines (– — –) to β-sheets ($J_{H^\alpha H^N} \sim 9$ Hz) and dashed lines to random-coil conformations ($J_{H^\alpha H^N} \sim 7$ Hz) (Wüthrich, 1986; Case et al., 1994). Plots (a), (c) and (e) treat the case of amino acids with only one β-proton (Ile, Thr and Val). In (a) and (c) the $J_{H^\alpha H^\beta}$ is set to 3.72 Hz and 12 Hz, respectively, which is within the range expected for single staggered χ_1 side-chain conformations (De Marco et al., 1978; West and Smith, 1998). Plot (e) shows the minimum (Ile) and maximum (Thr) attenuation factors expected for random-coil conformations based on the $J_{H^\alpha H^\beta}$ values reported by West and Smith (1998). Plots (b), (d) and (f) treat the case of amino acids with two β-protons (14 amino acids). In (b) the $J_{H^\alpha H^{\beta 2,3}}$ are both set to 3.72 Hz, while in (d) the $J_{H^\alpha H^{\beta 2,3}}$ are set to 3.72 and 12 Hz (De Marco et al., 1978; West and Smith, 1998). Plot (f) shows the minimum (Leu) and maximum (Ser) attenuation factors expected for random-coil conformations based on the $J_{H^\alpha H^\beta}$ values reported by West and Smith, 1998. Plot (g) shows the data calculated for Pro in a puckered down conformation (filled dots) and for Pro in a puckered up conformation (filled squares) (Cai et al., 1995). For the twist form of Pro, data are just the weighted average of those for the up and down forms (Cai et al., 1995). The other graphs in panel (g) refer to a Gly residue with non-degenerate H^α chemical shifts and the $J_{H^\alpha H^{\alpha'}}$ set to 15 Hz (Wüthrich, 1976). Plot (h) has been computed for an Ala residue setting all $J_{H^\alpha H^\beta}$ to 7 Hz (Wüthrich, 1976).

the window function employed to apodize the time domain FID (van de Ven, 1995; Cavanagh et al., 1996). However, an excessively long CT period (T) is not advisable in order to minimize water magnetization losses caused by chemical exchange. In addition, T can be fine tuned to optimize the channeling of the α-proton magnetization into antiphase coherences which do not lead to longitudinal magnetization during the NOE mixing time (Mori et al., 1996b; Otting, 1997). For this purpose, the term in the homonuclear coupling constant of Equation 1 has been computed for different amino acid types in several representative backbone and side-chain conformations as identified by recent statistical surveys (Cai et al., 1995; Chakrabarti and Pal, 1998; West and Smith, 1998) (Figure 2). As seen in Figure 2, for T of approximately 50 ms, homonuclear J couplings contribute a significant attenuation of α-proton magnetization for the majority of the cases. Furthermore, for the ^{13}C-labeled components eventually present, Equation 1 is multiplied by an additional $\cos(\pi {}^1J_{^{13}C^\alpha H^\alpha} T)$ factor which can be minimized by setting T equal to σ (1+2n) where $\sigma = (1/2{}^1J_{^{13}C^\alpha H^\alpha})$ and n is a positive integer. Moreover, the T dependence of terms representing scalar coupling in Equation 1 can be exploited to characterize NOEs arising from H^α protons, for instance by acquiring two spectra with different values of T (Mori et al., 1996b).

The CT-based filter benefits also from the advantages typical of non-selective experiments (Otting, 1997) such as the constructive use of t_1-noise and t_1-ridges for the identification of artifacts which would appear as subtraction errors when only selective water excitation is employed to filter water magnetization (Otting, 1997). Furthermore, the CT-block is not affected by the complications caused by negative excitation sidelobes which are sometimes observed for selective pulse shapes (Hajduk et al., 1993; Otting, 1997).

The Quadrature-Free (QF) approach – conceptual basis

A major drawback of experiments with an additional dimension, such as in the CT approach, is a loss of signal-to-noise ratio by a factor of $\sqrt{2}$ as compared to selective schemes. Besides, the sensitivity of pulse sequences with non-selective water excitation is even further compromised by difficulties in implementing water flip-back pulses because quadrature detection does not allow water magnetization to be longitudinal during the NOE mixing time for all FIDs (Otting, 1997). This limitation requires that long interscan delays are used to allow for water longitudinal relaxation unless relaxation agents are added to the solution (Otting, 1997). These problems can be overcome by introducing additional water selective pulses in the sequence (Gruschus and Ferretti, 1998, 1999) or by exploiting radiation damping (Lippens et al., 1995; Fulton and Ni, 1997). Here an alternative simple solution is presented which does not require any additional pulse and does not rely on radiation damping, thus maintaining water magnetization in well-defined and controlled states also during the mixing periods.

The CT-based experiment is dedicated to the investigation of water–macromolecule interactions and therefore the only signal of interest after the CT-filter is that of water itself. Water magnetization can be set to resonate at zero frequency offset relative to the proton channel carrier frequency and therefore no quadrature detection is indeed needed for the CT-t_1 evolution. The pulse sequence can for instance be written in the States-TPPI manner (Marion et al., 1989) and then the phase incrementation of the 90°(^{1}H) pulse pre-

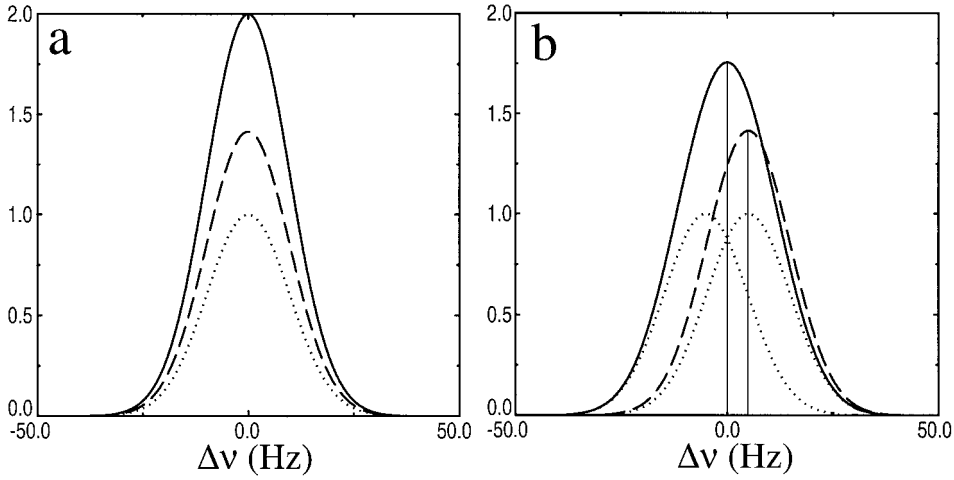

Figure 3. Effects of carrier frequency miscalibration on the water resonance. Dashed lines refer to the signal observed along ν_1 when quadrature detection (QD) is used to distinguish between positive and negative ν_1 offsets ($\Delta\nu$). The dashed signals are simulated using a representative Gaussian lineshape with a 23 Hz width-at-half-height and with peak intensity arbitrarily set to $\sqrt{2}$. Dotted lines indicate the signal components at two opposite frequency offsets into which the dashed resonance splits in the absence of QD. The sum of the dotted peaks is the signal observed when QD is not used and is shown with a solid line. The computation is performed for two representative carrier frequencies which always correspond to the point with $\Delta\nu = 0$. In case (a) the carrier frequency is correctly placed at the center of the water signal and therefore the two dotted lines overlap exactly, leading to a solid line signal enhanced by a factor of $\sqrt{2}$ as compared to the dashed QD peak. In case (b) the carrier frequency is misplaced at 5 Hz downfield relative to the center of the water signal. In this case the two dotted peak components at opposite $\Delta\nu$ do not overlap exactly and the resultant signal observed without QD (solid line) is frequency shifted and broadened relative to the dashed signal measured with QD. In case (b) the signal enhancement allowed by the elimination of QD is therefore less than the theoretical upper limit of $\sqrt{2}$ obtained in case (a).

ceding the CT-block can be eliminated (Figure 1). As shown by Figure 3a, this modification leads to a gain in signal-to-noise ratio by a factor of $\sqrt{2}$ and allows a facile implementation of the water flip-back strategy, which provides an additional gain in sensitivity without adding any relaxation agent to the solution. It should be noted that the efficiency of the 'quadrature-free' (QF) approach relies upon an accurate calibration of the proton carrier frequency in the middle of the water signal, as obtained for instance by optimizing the offset of a 50 ms long Gaussian 180° pulse in an e-PHOGSY (Dalvit and Hommel, 1995a; Dalvit, 1996) spin-echo on water of the type: 90°(^{1}H,hard)-Grad-180°(^{1}H,Gaussian)-Grad-Acquire. Figure 3b shows that when the proton carrier frequency is not correctly calibrated, the gain in the signal-to-noise ratio is less than the expected theoretical $\sqrt{2}$ factor.

The data set acquired with the QF approach can be processed as 'States' using NMRPipe (Delaglio et al., 1995). If only the receiver phase is inverted when t_1 is incremented (Figure 1a), the FT is executed with sign alternation. If not only the receiver phase but also the phase of the first ^{1}H pulse (and consequently that of the first water flip-back pulse; see Figure 1b) are inverted when t_1 is incremented, the FT is carried out without sign alternation. In both cases, after Fourier transform (FT) in NMRPipe a $-45°$ zero order phase correction is required in the ν_1 dimension provided that t_1 (Figure 1) for the first serial file is set to zero. The $-45°$ zero order phase correction originates because the complex data points are interpreted as having real and imaginary components of equal magnitude. After processing the 2D (Figure 1a) or 3D (Figure 1b) matrix, the row or the plane, respectively, corresponding to ν_1 = proton carrier frequency is extracted.

The exact ν_1 point number corresponding to the proton carrier frequency can be found after processing the multidimensional matrix by taking a vector along ν_1 at one of the edges where mainly only noise is present, executing inverse Fourier transform (FT), adding a large real constant and executing FT again to return to the frequency domain. A spike will appear at the carrier frequency (Wishart and Sykes, 1994). As an example, using NMRPipe (Delaglio et al., 1995) with zero filling to 2048 points, the carrier was found to correspond to point 1025, which coincides with the maximum of the water peak along ν_1. This is true for all test spectra recorded both with and without quadrature detection for ν_1, provided that the setting of the

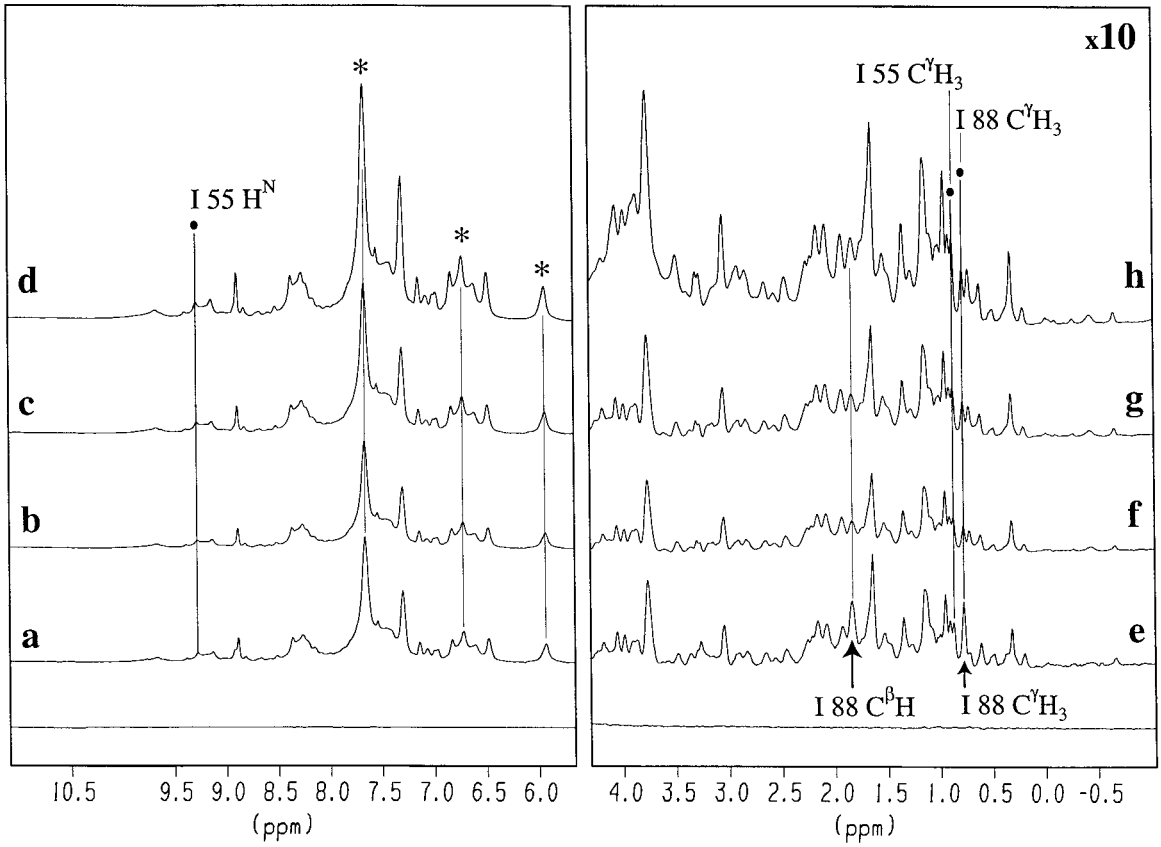

Figure 4. (a–d) Downfield and (e–h) upfield regions of water–protein NOE spectra of the HEWL sample at 36 °C. Panels (e–h) are vertically scaled by a factor of 10 relative to panels (a–d). All experiments were acquired on a DRX500 Bruker spectrometer using variants (see text) of the 2D sequence shown in Figure 1a and the following parameters. A spectral width of 8012.82 Hz was used for both dimensions. For t_1 and t_2, 350 and 1024 complex points were acquired, respectively, with 8 scans per FID. The length of the NOE mixing time was 52 ms. The inter-scan delay was 2 s, the number of dummy equilibration scans was 128, resulting in a total acquisition time per 2D spectrum of approximately 3 h and 40 min. For both dimensions a squared sinebell window function and zero filling to 2K points was applied. No water filter was employed during the processing. The 1D spectra shown in this figure are horizontal slices taken at ν_1 = proton carrier frequency (see text). Panels (a) and (e) derive from a 2D non-constant-time, quadrature detected experiment without water flip-back. Panels (b) and (f) are extracted from a 2D matrix acquired as the previous panels but with constant-time frequency labeling (Figure 1a). Panels (c) and (g) are water traces from a 2D experiment carried out as panels (b) and (f), but without quadrature detection. Panels (d) and (h) differ from (c) and (g) only for the introduction of the WFB pulse (Figure 1a). Dots indicate representative contributions from protein–water NOEs as previously assigned (Otting et al., 1997), while stars indicate representative contributions from chemical exchange between protein labile protons and water. Arrows denote representative contributions arising through NOE from H^{α} resonances close to the water signal.

carrier is calibrated as explained above. If the imaginary data is discarded after phasing, zero filling has to be executed at least up to the second higher power of 2 and Hilbert transform has to precede the inverse FT.

Materials

Hen egg-white lysozyme (HEWL) was purchased from Fluka AG, Switzerland, and was used as received to prepare a 9.4 mM sample in 500 μL of 90% ^1H_2O/ 10% ^2H_2O (*v/v*) at pH 3.8. Chymotrypsin inhibitor 2 (CI2) was generously made available by the Cambridge Centre for Protein Engineering (Medical Research Council, U.K.). Two CI2 samples were prepared, one uniformly ^{15}N-labeled and the other ($> \sim$20% ^{12}C, $< \sim$80%^{13}C), ^{15}N-labeled with proline residues significantly less than 80% ^{13}C-enriched. Both samples contain 7 mg of protein dissolved in 500 μL of a 90% ^1H_2O/ 10% ^2H_2O (*v/v*) 50 mM acetate buffer at pH 4.6.

Results and discussion

The 2D CT filter – implementation and validation

The ideas outlined above have been implemented in the pulse sequences shown in Figure 1a for unlabeled samples and in Figure 1b for samples which are ^{15}N-labeled and are either partially or non ^{13}C-labeled. The pulse sequence of Figure 1a will be discussed first. This 2D scheme was tested on the HEWL sample (Figure 4). The 1D spectra shown in Figure 4 are horizontal slices taken at ν_1 = proton carrier frequency.

The spectrum shown in Figures 4a and e serves as reference and was therefore acquired with the sequence of Figure 1a using States-TPPI quadrature detection (Marion et al., 1989) on ϕ_1 and without the water flip-back (WFB) pulse. In addition, the frequency labeling in t_1 is not constant-time: gradients G_2 were eliminated and the 180°(^{1}H) pulse with phase ϕ_2 was placed right before the second G_1 gradient. Another spectrum (Figures 4b and f) was then acquired using the same sequence employed for spectra (a) and (e), but with a 52 ms long constant-time t_1 evolution period as described in Figure 1a. In Figure 4 comparison of panels (a) and (e) versus (b) and (f), respectively, reveals that the peaks previously (Otting et al., 1997) ascribed to arise mainly from direct chemical exchange (stars) and from direct dipolar cross-relaxation (dots) with water are only minimally affected by the introduction of the CT period. The CT block preserves on the average more than 83% of the intensity of these signals; this percentage is expected to be even higher when more dilute (< 9.4 mM) solutions are used (Liepinsh and Otting, 1999). Besides, the CT significantly reduces contributions from $C^{\alpha}H$ protons resonating close to water, as shown by the arrows of Figure 4 for representative peaks which contain also a component arising through NOEs from the I88 $C^{\alpha}H$ proton resonating at 4.67 ppm (Kundrot and Richards, 1987; Redfield and Dobson, 1988).

The filtering properties of the CT block can also be clearly observed in Figures 5a and b, showing expanded 2D regions of spectra (a) and (b) of Figure 4, respectively: in the absence of CT (Figure 5a) the intermolecular cross peaks between water and protein protons are surrounded by a highly dense crowd of intramolecular cross peaks; in the presence of CT (Figure 5b) the intraprotein cross peaks are dramatically attenuated as the result of the synergetic effect of transverse (T_2) relaxation and of homonuclear scalar couplings (J). Together, the T_2 and the J filters are very effective, but a few cross peaks still remain in the region close to water (Figure 5b), highlighting the importance of combining these filters with the selection of a very narrow frequency band as allowed by high digital resolution along ν_1.

Finally, the relative efficiency of the relaxation and the scalar coupling filters can be appreciated by inspecting Figure 5c, which shows the expanded region of a spectrum acquired with the same sequence employed for Figure 5b but using a 4.2 ms Gaussian 180°(^{1}H) pulse in the CT period. This selective pulse causes the $\cos(\pi J_{ik}T)$ factors in Equation 1 to be replaced by $\cos(\pi J_{ik}t_1)$ terms, where the index *i* denotes a generic proton resonating close to water. Thus, in the spectrum of Figure 5c only the T_2 filter is effective, showing that transverse relaxation is not sufficient by itself to exclusively select water magnetization, therefore highlighting the importance of the homonuclear J filter effects.

The 2D QF-CT filter – implementation and validation

The above discussion illustrates the usefulness of the CT frequency labeling block for water filtering purposes. An additional advantage derives from the elimination of quadrature detection (vide supra), as demonstrated by panels (c) and (g) of Figure 4, which show the water trace of a 2D spectrum acquired with the same CT sequence used for spectra (b) and (f) but eliminating the 90° phase incrementation of ϕ_1. In order to facilitate the comparison of spectra acquired with and without quadrature detection, the difference spectrum between spectra (b) and (c), the latter scaled by a factor of $1/\sqrt{2}$, is reported below trace (a). Similarly, the difference spectrum between spectra (f) and (g), the latter scaled by a factor of $1/\sqrt{2}$, is reported below trace (e). The flatness of the difference spectrum clearly demonstrates that discarding quadrature detection does not introduce any significant artifact while increasing the signal-to-noise ratio by a $\sqrt{2}$ factor, as expected for an on-resonance water signal. Furthermore, as illustrated by Figures 4d and h, an additional gain in sensitivity is obtained through the implementation of the WFB strategy, which is facilitated by the elimination of quadrature detection. The observed gain in sensitivity resulting from the WFB pulse is $\geq$ 50% when the inter-scan delay is set to 2 s and it increases for shorter inter-scan delays.

The 3D QF-CT filter – implementation and validation

When a ^{15}N-labeled sample is available, the 3D pulse sequence of Figure 1b can be applied. A short spin-

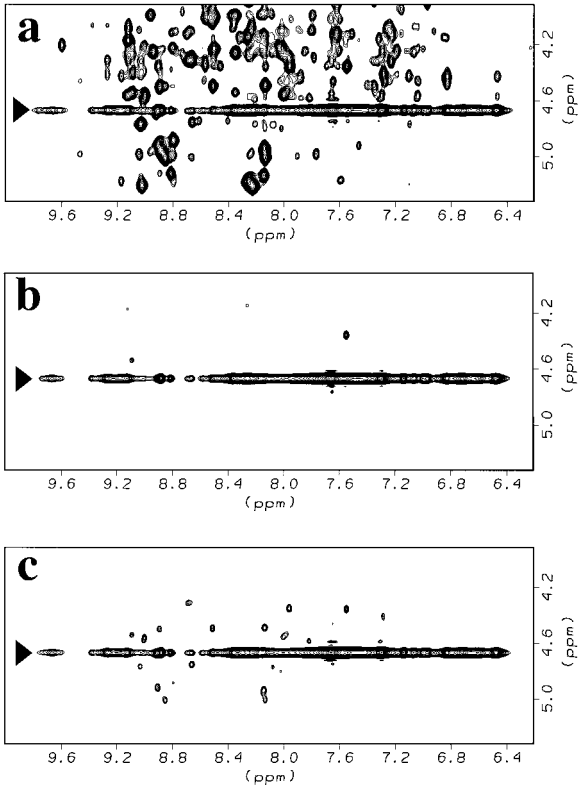

Figure 5. (a, b) Expanded regions of the 2D spectra corresponding to Figures 4a and b, respectively; (c) as (b) but acquired after replacing the 180°(^{1}H) hard CT pulse with a 180°(^{1}H) Gaussian of 4.2 ms long. All expansions are plotted with the same threshold, number of contour levels and level multiplier. Filled triangles indicate the position of the water row.

echo of the elegant e-PHOGSY type (Dalvit and Hommel, 1995a; Dalvit, 1996) is employed to decrease the spectral width needed in the t_1 dimension and achieve high digital resolution with only a small number of sampled t_1 points (Wagner and Wüthrich, 1979; Brüschweiler et al., 1987; Griesinger et al., 1987; Oschkinat et al., 1988; Kessler et al., 1989). The water flip-back HSQC block is essentially as previously described (Grzesiek and Bax, 1993a; Clore et al., 1994), except for the approach taken to decouple ^{13}C spins during ^{15}N evolution which follows Karimi-Nejad et al. (1999). The selection properties of this combined short e-PHOGSY/quadrature-free CT approach (Figure 1b) can be appreciated by comparison with the traditional single long and frequency selective e-PHOGSY spin-echo (Dalvit and Hommel, 1995a; Dalvit, 1996). For this purpose, the uniformly ^{15}N-labeled CI2 sample was employed.

Figure 6a displays the spectrum obtained using the sequence of Figure 1b in which the CT-block (see dashed box) was eliminated and the spin-echo extended to result in a 2D e-PHOGSY experiment (Dalvit and Hommel, 1995a) characterized by a 50.59 ms long 180° Gaussian pulse. This refocusing pulse decouples H^α protons resonating at the water frequency from amide and H^β protons. Therefore, in the e-PHOGSY spin-echo the filtering effect of homonuclear J is not exploited. In addition, H^α protons resonating at the water frequency spend on average approximately only half of the duration of the pulse as transverse magnetization, reducing also the filtering effects of the differential T_2 relaxation. Thus, the cross peaks in the spectrum of Figure 6a arise not only from interactions with water, such as the exchange peak of K21 (vide infra), but also from dipolar cross-relaxation with H^α protons resonating close to water, such as for instance the I48 H^α proton which is within NOE distance from I49 H^N. The cross peak of I49 appears therefore as an artifact in the e-PHOGSY-NOE-WFB-HSQC spectrum of Figure 6a. In contrast, this artifact is eliminated in the spectrum shown in Figure 6b, which was acquired in exactly the same time using the 3D QF-CT-based experiment of Figure 1b. This observation is also supported by Figure 6c, which contains an expansion of the rows through the cross peak of I49 in panels (a) and (b) (top and bottom, respectively). Other contributions arising from H^α protons are present in the spectrum of Figure 6a (see arrows), which are also reduced in the QF-CT experiment (Figure 6b).

The filtering efficiency of the sequence of Figure 1b does not significantly compromise the sensitivity of the experiment, as proved for CI2 by the minimal differences in signal-to-noise ratios observed between spectra (a) and (b) of Figure 6 for the cross peaks which arise from direct interactions with water, i.e. the peak of K21 (Figure 6d) which contains mainly contributions from chemical exchange with water, as indicated by a positive cross peak in the ROE spectrum (Figure 6e) acquired using the pulse sequence of Figure 1c.

Filtering water from mixtures of $^{13}C^\alpha H^\alpha$ and $^{12}C^\alpha H^\alpha$ protons

Finally, we address the issue of samples containing mixtures of unlabeled and ^{13}C-labeled components. Clearly, the QF-CT-filter discussed above (Figure 1a,b) can be applied to all H^α protons bound to both $^{12}C^\alpha$ and $^{13}C^\alpha$ carbon atoms. In addition,

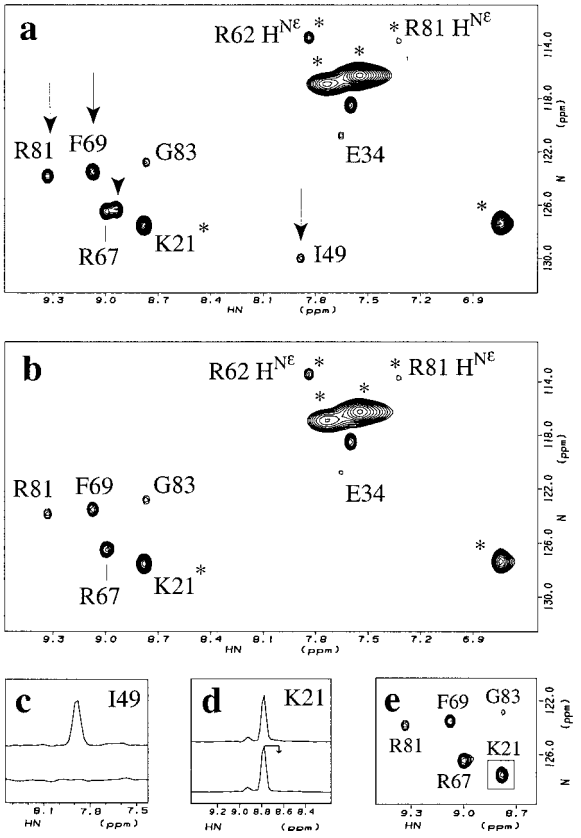

Figure 6. Water-protein H^N NOE spectra of the uniformly ^{15}N-labeled sample of CI2 at 27 °C. Experiments were performed at 500 MHz on a Bruker DRX500 spectrometer. Panel (a) shows the spectrum acquired using a 2D modification of the pulse sequence of Figure 1b, in which the CT block has been eliminated and the e-PHOGSY spin-echo (Dalvit and Hommel, 1995a; Dalvit, 1996) is executed with a 50.59 ms long Gaussian pulse. The gradients G_1 are set to the same strength as the weak gradients G_2 in Figure 1b and the strength and phase of the long Gaussian pulse were optimized to maximize the amount of refocused water magnetization. The total time between the two 90°(^{1}H) pulses preceding the NOE mixing time is therefore 52 ms, while $\tau_{mix} = 75.9$ ms. For the ^{15}N dimension 30 complex points were acquired using a spectral width of 1400 Hz. For the directly detected H^N dimension 512 complex points were recorded for a spectral width of 10000 Hz. An interscan delay of 1 s was used with 128 dummy scans and $560 = 140 \times 4$ scans. The residual water peak was convolution filtered prior to processing. Phase-shifted squared sinebell apodization functions were used in both dimensions and zero filling to 1K and 128 complex points was applied for t_1 and t_2, respectively. The ^{15}N dimension was indirectly referenced (Wishart et al., 1995). The arrows indicate representative contributions arising through NOE with H^α protons resonating close to the water signal (Kjaer et al., 1987; McPhalen and James, 1987). The stars denote cross peaks containing mainly contribution from chemical exchange with water magnetization as proved by NOE/ROE comparison (see panel (e) and Figure 7c). All peaks with a star but K21 are aliased one or more times. Amino acid labels indicate residue assignments based on ^{15}N-separated TOCSY and NOESY spectra and previous assignments (Kjaer et al., 1987). Panel (b) shows a spectrum acquired using the pulse sequence of Figure 1b which combines a short e-PHOGSY spin-echo (180° Gaussian of 4.04 ms) with a CT period of 46.55 ms. The total time between the two 90°(^{1}H) pulses preceding the NOE mixing time is therefore still 52 ms, as for the classical e-PHOGSY experiment of panel (a). Using 70 complex t_1 points for a spectral width of 1602.6 Hz, 4 scans and keeping all other parameters as for the spectrum of panel (a) resulted in exactly the same acquisition time as for the e-PHOGSY experiment (a): 13 h, 48 min, 51 s. The processing of the HSQC planes of this 3D experiment was as for the e-PHOGSY spectrum (a) and for t_1 a 90° phase shifted squared sinebell with zero filling to 256 complex points was applied. Panel (b) shows the HSQC plane corresponding to the proton carrier frequency, which was found as described in the text. Symbols have the same meaning as in panel (a). In panel (c) upper and lower spectra correspond to traces through the cross peak of I49 in spectra (a) and (b), respectively. In panel (d) upper and lower spectra correspond to traces through the cross peak of K21 in spectra (a) and (b), respectively. The arrow indicates the ranges of relative intensities obtained by repeating the experiments, also using different truncation levels and/or number of points for the Gaussian pulses. Panel (e) shows an expansion of the ROE version of spectrum (b), acquired according to Figure 1c and processed as spectrum (b).

for the fraction of H^α protons connected to $^{13}C^\alpha$ the simultaneous isotope filter can be also exploited as implemented in the experiment schematized in Figure 1b. The sequence of Figure 1b was applied to the sample of ($> \sim$20% ^{12}C, $< \sim$80% ^{13}C),^{15}N-labeled CI2, intentionally using a relatively short (17.5 ms) CT period in order to critically test the isotope filter. When $^{13}C^\alpha$ spins are decoupled by CPD the water-NOE spectrum contains as well many cross peaks arising from H^α protons rather than from water, as for instance the cross peak of I49 (Figure 7a). When instead the isotope filter is applied, the artifacts caused by $^{13}C^\alpha$-bound protons are attenuated (Figure 7b).

The inset of Figure 7b illustrates that the isotope filter cannot by itself completely eliminate artifacts originating from H^α protons because of the incomplete ^{13}C labeling. Moreover, the Pro residues are only minimally ^{13}C labeled leading to significant residual H^α contributions in the isotope-filtered spectrum (Figure 7b, see arrows). It is therefore advisable to revert to experiments acquired as explained for Figure 6, with longer CT periods and higher digital resolution. The pulse sequence of Figure 1b then combines efficiently and synergistically four effects which contribute to the clean selection of water magnetization: frequency selection, differential relaxation, antiphase defocusing by homo- and heteronuclear scalar coupling.

A further filtering effect can be added to the experiment of Figure 1b if the mixing period is adapted

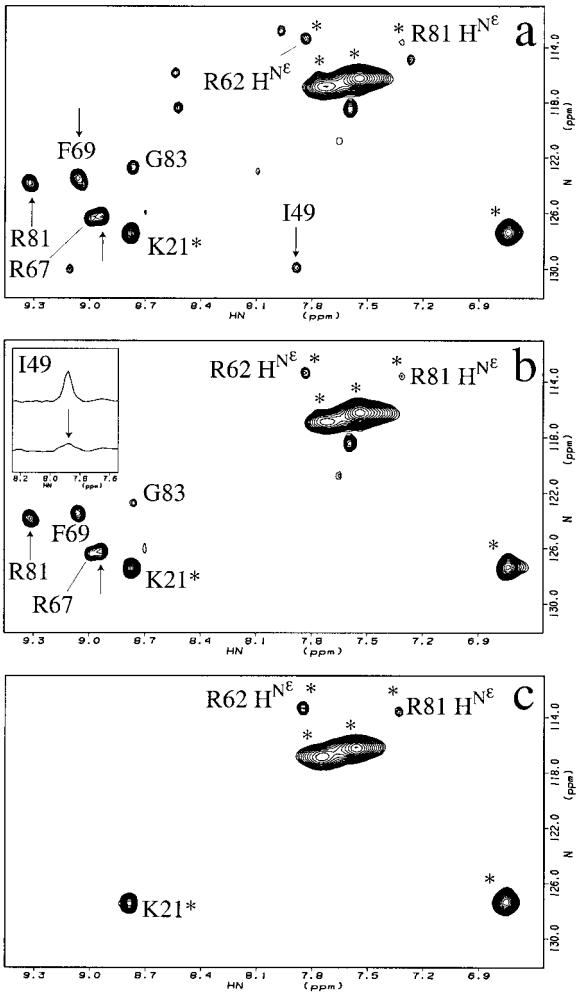

Figure 7. Water–protein H^N NOE spectra of a ^{15}N-labeled sample of CI2 only partially ^{13}C enriched (see Materials section). Experiments were performed at 27 °C and 500 MHz on a Bruker DRX500 spectrometer. Panel (a) shows the spectrum acquired with the pulse sequence of Figure 1b in which the first two ^{13}C pulses were eliminated and ^{13}C composite-pulse-decoupling (CPD) was applied throughout the CT period when gradients were absent. In order to reliably test the efficiency of the isotope filter in purging the NOEs originating from H^α magnetization, a short CT period (17.5 ms) was used with only 4 complex points for a spectral width of 1602.6 Hz. An interscan delay of 1 s and 16 scans were employed. Panel (b) shows a spectrum acquired as (a) but without CPD (Figure 1b). In the inset upper and lower spectra correspond to traces through the cross peak of I49 in spectra (a) and (b), respectively. Panel (c) shows the off-resonance ROE version ($\theta = 35.5°$) of (b) acquired with 8 complex points for t_1, a CT block 45.5 ms long and 8 scans. Acquisition parameters which are not mentioned here remained as for the experiments in Figure 6b. The processing was carried out similarly as described in Figure 6b and symbols also have the same meaning as in Figure 6. All panels are displayed with the same threshold and plotting parameters.

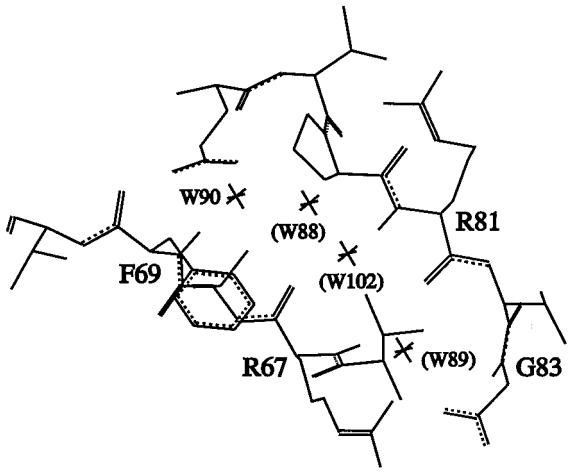

Figure 8. Two antiparallel pseudo β-sheet strands of the X-ray determined structure of CI2 (2ci2, McPhalen and James, 1987), showing the water molecules which account for the observed NOEs in solution. Not all the water molecules indicated within brackets are necessary to explain the detected cross peaks to H^N of R67 and R81 (see text).

to off-resonance ROE transfer characterized by an effective tilt of 35.5° (Figure 1d and Figure 7c). This angle results in NOE/ROE cancellation of the cross peaks which arise from dipolar cross-relaxation with $\omega\tau_c \gg 1$ (Birlirakis et al., 1996). The peaks observed in Figure 7c for the 35.5° off-resonance ROE spectrum arise instead mainly from chemical exchange with water. This observation is also supported by direct comparison of NOE and on-resonance ROE spectra. Other mixing blocks, for instance for exchange-relay editing (Hwang et al., 1997; Dalvit, 1998; Melacini et al., 1999a, b; Phan et al., 1999), can be similarly incorporated in the pulse sequence of Figure 1b.

Hydration of CI2

Inspection of the ROE spectrum (Figure 6e) reveals negative ROE/NOE ratios for the H^N protons of R67, F69, R81 and G83, indicating that these cross peaks contain mainly contributions either from direct intermolecular NOEs with water protons or from intramolecular NOEs exchange-relayed by labile protein protons (Otting, 1997). Using an NOE cut-off distance of 4.5 Å and the X-ray structure 2ci2 (McPhalen and James, 1987), the latter case was ruled out for the H^N protons of R67, F69, R81. The observed NOEs to these H^N are instead fully accounted for by the X-ray detected water molecule oxygen atoms (McPhalen and James, 1987): W88 is within 3.7 Å from the H^N of R81, W89 is within 2.1 Å from the H^N of R67, W90 is within 2.0 Å from the H^N of F69, W102 is within

3.8 Å from the H^N of R67 and within 2.2 Å from the H^N of R81. These water molecules are conserved in nine other X-ray structures, including CI2 mutants (PDB codes: 1coa (Jackson et al., 1993), 1cq4, 1ypa, 1ypb, 1ypc), CI2 fragments (PDB code 1ciq) and CI2 complexed with subtilisins (PDB codes 1a1o, 1a1y, 2sni (McPhalen and James, 1988)) and they are part of a spine of hydration between two antiparallel pseudo β-strands (Figure 8). Moreover, according to the definition of Lee and Richards (1978), the X-ray structure of CI2 indicates that these four water molecules are buried (McPhalen and James, 1987), in full agreement with the negative observed NOE/ROE ratios (vide supra).

These observations solve some inconsistencies previously reported for the NMR refined structure of CI2 (Ludvigsen et al., 1991), in which not all the backbone-to-backbone NOEs expected for direct hydrogen bonds between the β-strands 65–67 and 81–83 matched the experimental data. In addition, the presence of inter-strand water molecules was also previously suggested based on molecular dynamics simulations (Nanzer et al., 1994; Li and Daggett, 1995).

Conclusions

The proposed CT pulse sequence allows to select water magnetization with enhanced specificity through a synergetic combination of several separation principles, including relaxation, frequency, homo- and hetero-nuclear scalar coupling filters. Furthermore, the introduction of the QF approach results in a $\sqrt{2}$ gain in signal-to-noise ratio and facilitates the implementation of water flip-back pulses, leading, in the tested cases, to a sensitivity comparable to that obtained with selective water excitation schemes. This methodology enabled to investigate the hydration of a CI2 sample which was only partially ^{13}C-enriched, providing evidence for water molecules in a hydration spine between two pseudo β-sheet strands and highlighting the potential of the proposed experiment for hydration studies of mixtures containing labeled and unlabeled components such as ligand–macromolecule complexes.

Acknowledgements

We thank Prof. A. Fersht and Mr. N.W. Foster (Cambridge Centre for Protein Engineering, Medical Research Council, U.K.) for generously making CI2 available. The authors are indebted to Ing. Albert George for the preparation of CI2 samples and for helpful discussions, to Ing. Nico Zwanenburg and to Ing. Johan van der Zwan for expert technical assistance. Dr. Marco Tessari is gratefully acknowledged for insightful discussions.

References

Bax, A., Mehlkopf, A.F. and Smidt, J. (1979) *J. Magn. Reson.*, **35**, 167–169.
Bax, A. and Freeman, R. (1981) *J. Magn. Reson.*, **44**, 542–561.
Birlirakis, N., Cerdan, R. and Guittet, E. (1996) *J. Biomol. NMR*, **8**, 487–491.
Böckmann, A. and Guittet, E. (1996) *J. Biomol. NMR*, **8**, 87–93.
Brüschweiler, R., Madsen, J.C., Griesinger, C., Sørensen, O.W. and Ernst, R.R. (1987) *J. Magn. Reson.*, **73**, 380–385.
Cai, M., Huang, Y., Liu, J. and Krishnamoorthi, R. (1995) *J. Biomol. NMR*, **6**, 123–128.
Case, D.A., Dyson, H.J. and Wright, P.E. (1994) *Methods Enzymol.*, **239**, 392–416.
Cavanagh, J., Fairbrother, W.J., Palmer III, A.G. and Skelton, N.J. (1996) *Protein NMR Spectroscopy. Principle and Practice*, Academic Press, San Diego, CA.
Chakrabarti, P. and Pal, D. (1998) *Protein Eng.*, **11**, 631–647.
Clore, G.M., Bax, A., Omichinski, J.G. and Gronenborn, A.M. (1994) *Structure*, **2**, 89–94.
Dalvit, C. (1995) *J. Magn. Reson.*, **A113**, 120–125.
Dalvit, C. and Hommel, U. (1995a) *J. Magn. Reson.*, **B109**, 334–338.
Dalvit, C. and Hommel, U. (1995b) *J. Biomol. NMR*, **5**, 306–311.
Dalvit, C. (1996) *J. Magn. Reson.*, **B112**, 282–288.
Dalvit, C. (1998) *J. Biomol. NMR*, **11**, 437–444.
Delaglio, F., Grzesiek, S., Vuister, G.W., Zhu, G., Pfeifer, J. and Bax, A. (1995) *J. Biomol. NMR*, **6**, 277–293.
De Marco, A., Llinas, M. and Wüthrich, K. (1978) *Biopolymers*, **17**, 617–636.
Desvaux, H. and Goldman, M. (1996) *J. Magn. Reson.*, **B110**, 198–201.
Fulton, D.B. and Ni, F. (1997) *J. Magn. Reson.*, **129**, 93–97.
Gemmecker, G., Jahnke, W. and Kessler, H. (1993) *J. Am. Chem. Soc.*, **115**, 11620–11621.
Griesinger, C., Sørensen, O.W. and Ernst, R.R. (1987) *J. Magn. Reson.*, **73**, 574–579.
Gruschus, J.M. and Ferretti, J.A. (1998) *J. Magn. Reson.*, **135**, 87–92.
Gruschus, J.M. and Ferretti, J.A. (1999) *J. Magn. Reson.*, **140**, 451–459.
Grzesiek, S. and Bax, A. (1993a) *J. Biomol. NMR*, **3**, 627–638.
Grzesiek, S. and Bax, A. (1993b) *J. Am. Chem. Soc.*, **115**, 12593–12594.
Hajduk, P.J., Horita, D.A. and Lerner, L.E. (1993) *J. Magn. Reson.*, **A103**, 40–52.
Hwang, T.L., Mori, S., Shaka, A.J. and van Zijl, P.C.M. (1997) *J. Am. Chem. Soc.*, **119**, 6203–6204.
Jackson, S.E., Moracci, M., Elmasry, N., Johnson, C.M. and Fersht, A.R. (1993) *Biochemistry*, **32**, 11259–11266.
Karimi-Nejad, Y., Löhr, F., Schipper, D., Rüterjans, H. and Boelens, R. (1999) *Chem. Phys. Lett.*, **300**, 706–712.

Kessler, H., Anders, U., Gemmecker G. and Steuernagel, S. (1989) *J. Magn. Reson.*, **85**, 1–7.
Kjaer, M., Ludvigsen, S., Sørensen, O.W., Denys, L.A., Kindtler, J. and Poulsen, F.M. (1987) *Carlsberg Res. Commun.*, **52**, 327–354.
Kriwacki, R.W., Hill, R.B., Flanagan, J.M., Caradonna, J.P. and Prestegard, J.H. (1993) *J. Am. Chem. Soc.*, **115**, 8907–8915.
Kundrot, C.E. and Richards, F.M. (1987) *J. Mol. Biol.*, **193**, 157–175.
Lee, B. and Richards, F.M. (1978) *J. Mol. Biol.*, **55**, 379–387.
Li, A. and Daggett, V. (1995) *Protein Eng.*, **8**, 1117–1128.
Liepinsh, E. and Otting, G. (1999) *J. Biomol. NMR*, **13**, 73–76.
Lippens, G., Dhalluin, C. and Wieruszeski, J.M. (1995) *J. Biomol. NMR*, **5**, 327–331.
Ludvigsen, S., Shen, H., Kjaer, M., Madsen, J.C. and Poulsen, F.M. (1991) *J. Mol. Biol.*, **222**, 621–635.
Marion, D., Ikura, M., Tschudin, R. and Bax. A. (1989) *J. Magn. Reson.*, **85**, 393–399.
McPhalen, C.A. and James, M.N.G. (1987) *Biochemistry*, **26**, 261–275.
McPhalen, C.A. and James, M.N.G. (1988) *Biochemistry*, **27**, 6582–6590.
Melacini, G., Kaptein, R. and Boelens, R. (1999a) *J. Magn. Reson.*, **136**, 214–218.
Melacini, G., Boelens, R. and Kaptein, R. (1999b) *J. Biomol. NMR*, **13**, 67–71.
Mori, S., Johnson, M.O., Berg, J.M. and van Zijl, P.C.M. (1994) *J. Am. Chem. Soc.*, **116**, 11982–11990.
Mori, S., Abeygunawardana, C., van Zijl, P.C.M. and Berg, J.M. (1996a) *J. Magn. Reson.*, **B110**, 96–100.
Mori, S., Berg, J.M. and van Zijl, P.C.M. (1996b) *J. Biomol. NMR*, **7**, 77–82.
Nanzer, A.P., Poulsen, F., van Gunsteren, W.F. and Torda, A.E. (1994) *Biochemistry*, **33**, 14503–14511.
Oschkinat, H., Clore, G.M. and Gronenborn, A.M. (1988) *J. Magn. Reson.*, **78**, 371–375.
Otting, G. and Wüthrich, K. (1989) *J. Am. Chem. Soc.*, **111**, 1871–1875.
Otting, G., Liepinsh, E. and Wüthrich, K. (1991a) *Science*, **254**, 974–980.
Otting, G., Liepinsh, E., Farmer II, B.T. and Wüthrich, K. (1991b) *J. Biomol. NMR*, **1**, 299–305.
Otting, G. (1994) *J. Magn. Reson.*, **B103**, 288–291.
Otting, G. and Liepinsh, E. (1995a) *J. Biomol. NMR*, **5**, 420–425.
Otting, G. and Liepinsh, E. (1995b) *J. Magn. Reson.*, **B107**, 192–198.
Otting, G. (1997) *Progr. NMR Spectrosc.*, **31**, 259–285.
Otting, G., Liepinsh, E., Halle, B. and Frey, U. (1997) *Nat. Struct. Biol.*, **4**, 396–404.
Phan, A.T., Leroy, J.L. and Guéron, M. (1999) *J. Mol. Biol.*, **286**, 505–519.
Pitner, T.P., Glickson, J.D., Dadok, J., Bothner-By, A.A. and Roderich, W. (1974) *Nature*, **250**, 582–584.
Rance, M., Wagner, G., Sørensen, O.W., Wüthrich, K. and Ernst, R.R. (1984) *J. Magn. Reson.*, **59**, 250–261.
Redfield, C. and Dobson, C.M. (1988) *Biochemistry*, **27**, 122–136.
Santoro, J., Bruix, M., Gonzalez, C., Nieto, J.L. and Rico, M. (1992) *J. Biomol. NMR*, **2**, 647–653.
Sklenar, V., Piotto, M., Leppik, R. and Saudek, V. (1993) *J. Magn. Reson.*, **A102**, 241–245.
Sklenar, V. (1995) *J. Magn. Reson.*, **A114**, 132–140.
Stejskal, E.O. and Tanner, J.E. (1965) *J. Chem. Phys.*, **42**, 288–292.
Van de Ven, F.J.M. (1995) *Multidimensional NMR in Liquids*, VCH, New York, NY.
Van de Ven, F.J.M. and Philippens, M.E.P. (1992) *J. Magn. Reson.*, **97**, 637–644.
Vuister, G.W. and Bax, A. (1992) *J. Magn. Reson.*, **98**, 428–435.
Wagner, G. and Wüthrich, K. (1979) *J. Magn. Reson.*, **33**, 675–680.
West, N.J. and Smith, L.J. (1998) *J. Mol. Biol.*, **280**, 867–877.
Wider, G., Riek, R. and Wüthrich, K. (1996) *J. Am. Chem. Soc.*, **118**, 11629–11634.
Wishart, D.S. and Sykes, B.D. (1994) *Methods Enzymol.*, **239**, 363–392.
Wishart, D.S., Bigam, C.G., Yao, J., Abildgaard, F., Dyson, J.H., Oldfield, E., Markley, J.L. and Sykes, B.D. (1995) *J. Biomol. NMR*, **6**, 135–140.
Wüthrich, K. (1976) *NMR in Biological Research: Peptides and Proteins*, Elsevier Inc., New York, NY.
Wüthrich, K. (1986) *NMR of Proteins and Nucleic Acids*, John Wiley, New York, NY.